

10-13-2020

Investigation of mode I-II-III fracture of brittle spheres with a 60° internal crack using 3D-ILC

Hai-jun WANG

State Key Laboratory of Hydrology-Water Resource and Hydraulic Engineering, Nanjing Hydraulic Research Institute, Nanjing, Jiangsu 210029, China

Shu-yang YU

Collaborative Innovation Center on Water Safety and Water Science, Hohai University, Nanjing, Jiangsu, 210098, China

Zi-xuan TANG

State Key Laboratory of Hydrology-Water Resource and Hydraulic Engineering, Nanjing Hydraulic Research Institute, Nanjing, Jiangsu 210029, China

Lei TANG

State Key Laboratory of Hydrology-Water Resource and Hydraulic Engineering, Nanjing Hydraulic Research Institute, Nanjing, Jiangsu 210029, China, leitang@nhri.cn

See next page for additional authors

Follow this and additional works at: <https://rocksoilmech.researchcommons.org/journal>



Part of the [Geotechnical Engineering Commons](#)

Custom Citation

WANG Hai-jun, YU Shu-yang, TANG Zi-xuan, TANG Lei, REN Ran, XU Jin, . Investigation of mode I-II-III fracture of brittle spheres with a 60° internal crack using 3D-ILC[J]. Rock and Soil Mechanics, 2020, 41(5): 1573-1582.

This Article is brought to you for free and open access by Rock and Soil Mechanics. It has been accepted for inclusion in Rock and Soil Mechanics by an authorized editor of Rock and Soil Mechanics.

Investigation of mode I-II-III fracture of brittle spheres with a 60° internal crack using 3D-ILC

Authors

Hai-jun WANG, Shu-yang YU, Zi-xuan TANG, Lei TANG, Ran REN, and Jin XU

Investigation of mode I-II-III fracture of brittle spheres with a 60° internal crack using 3D-ILC

WANG Hai-jun¹, YU Shu-yang², TANG Zi-xuan¹, TANG Lei¹, REN Ran³, XU Jin⁴

1. State Key Laboratory of Hydrology-Water Resource and Hydraulic Engineering, Nanjing Hydraulic Research Institute, Nanjing, Jiangsu 210029, China

2. Collaborative Innovation Center on Water Safety and Water Science, Hohai University, Nanjing, Jiangsu, 210098, China

3. Huatian Corporation, China Metallurgical Group Corporation, Nanjing, Jiangsu 210019, China

4. Ecole Nationale Supérieure de Techniques Industrielles et des Mines de Douai, Douai, France, 59500

Abstract: As one of the perfect geometries in nature, sphere is common in daily and industrial life. The mechanical properties of sphere are of great significance to engineering safety and numerical simulation. Internal cracks or defects are inherent properties of materials and have an important influence on the mechanical properties of materials. However, the internal crack of the sphere is not considered in the current research due to the limit of technology. Thus, understanding of the propagation of internal cracks of brittle spheres is limited. In our study, internal cracks were created in glass sphere samples by 3D-ILC (3D-internal laser-engraved crack). Uniaxial compression tests were performed on samples with an internal crack at 60°. By comparing with results of intact sphere samples, the propagation of the internal crack, the load and the fractography were investigated. The distributions of K_I , K_{II} , K_{III} were calculated using M-integral. Results shows that: 1) the fracture patterns include wing cracks and primary crack; 2) the wing crack is composed of the smooth zone (mode I-II fracture) and the tear zone (mode I-II-III fracture); 3) the distributions of K_I , K_{II} , K_{III} around crack tips obtained by M-integral are consistent with the test results; 4) 3D-ILC can be successfully applied into the investigation of internal cracks of spheres and it provides experimental and theoretical basis for the study of 3D problem, internal cracks, and mode I-II-III fracture in fracture mechanics of brittle materials.

Keywords: transparent rock-like materials; 3D internal crack; 3D-ILC; fracture mechanics; sphere

1 Introduction

As one of the perfect geometries in nature, sphere is also common in the daily and industrial life. Minerals in nature, explosives in industrial productions^[1], rock-fills in civil and hydraulic engineering^[2], seepage proof material for the core wall, landfill final covers^[3] and so on are composed of numerous particles. Due to the exact mathematical description of sphere, researchers always regard these particles as a sphere^[4]. The sphere is used as a unit in the discrete element numerical algorithm in geotechnical engineering such as PFC^{3D}. Therefore, having a good understanding of the physical and mechanical properties of the sphere is of great significance to engineering & disaster prevention and numerical simulation^[5].

There have been several investigations about spherical particles and our study focused on the characteristics of cracks in the brittle spheres. Xavier et al.^[6] investigated the crack initiation and monitored the

cracking pattern by different tests including quasistatic compression of glass spheres and edge-on-impacts. Salman et al.^[7] displayed the forms of failure in soda-lime glass spheres and found their variations with different sphere diameters and impact velocities in impact and compression tests. Pernas-sánchez et al.^[8] analyzed the ice impact process on a rigid plate in tests and found that the fragmentation process of the ice behaved as an agglomeration of particles. In theory, Shen et al.^[4] investigated the evolution for the particle failure of granular materials from a mesomechanical and thermodynamic insight. Cheong et al.^[9] modelled the fragment size distribution by a two-parameter Weibull distribution equation and obtained the threshold conditions for the transition. Shi et al.^[10] and Zhu et al.^[11] used peridynamics (PD) to simulate the initiation, nucleation and fracture characteristics of granular materials under different loading conditions. The process of initiation, propagation and breakage of crack for quasi-brittle spheres was modelled using the combined finite

Received: 17 June 2019

Revised: 12 September 2019

This work was supported by the National Key Research and Development Plan(2016YFC0401801), the National Natural Science Foundation of China (51409170,51739008,U1765204) and the Natural Science Foundation of Jiangsu Province(BK20171130).

First author: WANG Hai-jun, male, born in 1985, PhD, Supervisor for master students, Senior engineer, focusing on fracture mechanics of rocks.

E-mail: hjwang@nhri.cn

Corresponding author: TANG Lei, male, born in 1971, PhD, Professor-level senior engineer, focusing on structural engineering. E-mail: leitang@nhri.cn

and discrete element method (FDEM) by Ma et al.^[12] and Chen et al.^[13].

Internal cracks or defects are inherent properties of materials and have an important influence on the mechanical properties of materials^[14]. However, the internal crack of sphere is not considered in the research mentioned above. Understanding of the propagation of internal cracks of brittle spheres is still limited at present, and the internal crack itself is one of the difficulties in the fracture mechanics of the brittle solid. The internal crack is always inside the solid and it is difficult to observe. Therefore, a transparent material is usually used in tests. Additionally, it is hard to generate internal cracks that meet the test requirements within the sphere. Currently, there are three methods for creating the internal cracks: (1) Cut and cement^[15]: two blocks of polymethylmethacrylate plastic (PMMA) with surface cracks are cemented together and the surface cracks are regarded as internal cracks. Obviously, this method cannot maintain the integrity of the sample. (2) Embed and cast^[16]: metal or mica sheet is put into the mold and then pour the resin to form, and these thin inclusions embedded during casting are treated as the internal cracks. This method is commonly adopted for modelling the internal cracks in transparent rock-like materials by many scholars and many achievements have been made during the recent five years^[17–20]. However, the brittleness index of the sample obtained by this method is 1/3–1/7 under the test condition with low temperature, and the brittleness index for rocks is 1/12–1/35. Meanwhile, mica or metal still has a difference from real cracks. (3) Promising 3D printing: Ju et al.^[21] made a natural coal rock model with complex fractures, and Liu^[22] obtained transparent rock-like models using this method. There are some advantages of 3D printing. It is not necessary to use cotton threads to hold the metal or mica, and the internal crack or joint morphology can be easily controlled. Moreover, the efficiency of production has been improved. However, it still has some drawbacks. The brittleness of samples made of resin or photosensitive materials is far from that of rocks and the printed internal crack is a cavity instead of a fracture caused by mechanical factors. Additionally, it is challenging and expensive to print transparent brittle materials of

high quality.

To solve the problems mentioned above, the internal cracks in this study are generated in glass spheres using our proposed 3D-ILC (3D-internal laserengraved crack) technology. The distributions of K_I , K_{II} , K_{III} are obtained by analysis of failure mode and fracture morphology in tests, which are also compared with results calculated by theoretical methods. Results in our study can provide an experimental and theoretical basis for the investigation of 3D problem, internal cracks and mode I-II-III fracture in fracture mechanics of brittle materials.

2 Sample preparation and testing methods

2.1 3D-ILC

The 3D-ILC technology was proposed by Wang et al.^[23] in 2017. The laser is used in this technology to penetrate the object and create the internal crack without damage to the surface instead of destroying the solid surface to create the internal crack like traditional methods. The main difference between the 3D-ILC and previous methods lies in the formation of a smooth fatigue crack propagation ring, due to the thermal shock of the high-frequency laser. At present, this technique has been successfully applied to the study of the orifices with internal cracks^[24], the cracking propagation characteristics of the Brazilian discs^[25] and three-point bending^[26]. The details of this technology will not be introduced here.

2.2 Testing materials

Glass is chosen as the testing material in this study. In the book "Introduction to Rock Fracture Mechanics", Li^[27] demonstrated the prevalence of glass in solid mechanics: "Glass is used in all pioneering tests of solid mechanics, including fracture mechanics." The foundations of fracture mechanics conducted by Griffith is also studied using glass^[28].

The advantages of glass are as follows: (a) it is the most continuous, uniform, isotropic, linear elastic, and brittle material at room temperature^[29]. As a classic brittle testing material in solid mechanics, it eliminates the interference of various complex factors, and can be used as an alternative testing material for both non-metallic and metallic brittle materials such as rock, ceramics, cement, and cast iron; (b) brittleness is currently

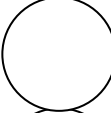
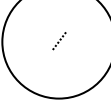
the most important indicator of rock-like materials. The tension-compression ratio of rock is in the range of 1/12–1/35, while that of glass is 1/13–1/33. Glass is closer to rock than the current mainstream materials, in terms of brittleness; (c) glass is a photochromic material with stress birefringence, which provides a basis for the visualization of the internal stress field; (d) the glass production technology is very mature and prevalent, and it can be easily modified. Moreover, there is no technical barrier to produce porous or granular glass. Combined with 3D-ILC, it provides advantages for the study of internal cracks in porous media; (e) the

glass fractures have typical characteristics; thus, it provides a foundation for the application of fracture theory.

2.3 Testing schemes

In order to study the fracture characteristics of a sphere with three-dimensional internal cracks under uniaxial compression, two samples were used for testing: samples without original internal cracks induced by 3D-ILC (control group A), and samples containing original internal cracks (test group B). The sample numbers, loading schemes and contents to be analyzed are shown in Table 1.

Table 1 Test schemes and sample No.

Sample category	Sample number	Schematic diagram	Purpose	Contents to be analyzed					
				Stress moire	Failure mode	Crack characteristics	Crack fractography	Propagation rate	Numerical analysis
Control group	A1		Compare with the test group B	√	√	×	×	×	×
	A2			√	√	×	×	×	×
	A3			√	√	×	×	×	×
	A4			√	√	×	×	×	×
Test group	B1		Observe the failure process of samples	√	√	√	√	√	√
	B2			√	√	√	√	√	√
	B3			√	√	√	√	√	√
	B4			√	√	√	√	√	√

Note: √ represents the contents which are analyzed in this study, and × indicates the contents that are not analyzed.

(1) Control group A: samples without internal cracks induced by 3D-ILC, are used to provide comparative data for group B—spherical samples with internal cracks. The sample numbers are from A1 to A4.

(2) Test group B (crushing group): spherical samples with internal cracks of 60° are completely damaged by load. The internal crack propagation and the characteristic of load will be focused on during the process. The sample numbers are from B1 to B4.

2.4 Sample preparation

(1) Group A: As shown in Fig.1, the sample is a sphere with a diameter of 80 mm. The samples in this group provide comparisons for the samples with internal cracks.

(2) Group B: As shown in Fig.2, the sample is a sphere with an original internal crack induced by 3D-ILC and has a diameter of 80 mm. The internal crack is circular with a diameter of about 15 mm, and the center of the circle is located at the center of the sphere with an angle of 60° to the horizontal direction.

2.5 Testing apparatus

The WHY-3000 servo loading system is used in this test, with the uniaxial compression load and the

force control mode, and has a rate of 0.02 kN/s. Cameras are set at different angles to monitor the crack initiation, dynamic change of the crack propagation and failure process. The flashlight is used to adjust the sample's light. The arrangement of test instruments is shown in Fig. 3.

The brittleness test is relatively sensitive to the stress concentration, and the roughness can lead to cracks at the tips of the sample, which affects the quality of the test. To address this issue, smooth PMMA plates (plastic plates) of the same size and thickness (5 mm) are placed at the top and bottom.

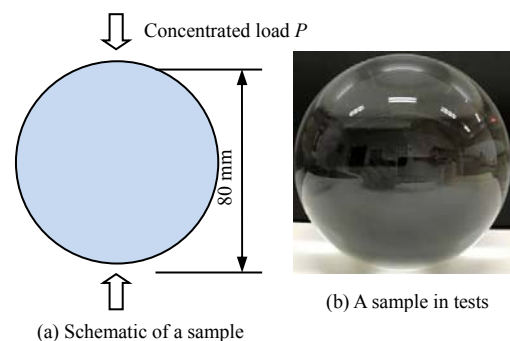


Fig.1 Sphere without crack (group A)

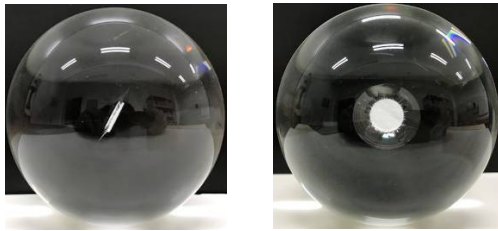
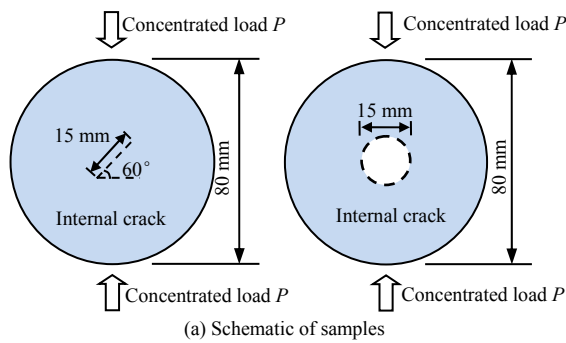


Fig.2 Sphere with 3D internal crack (group B)

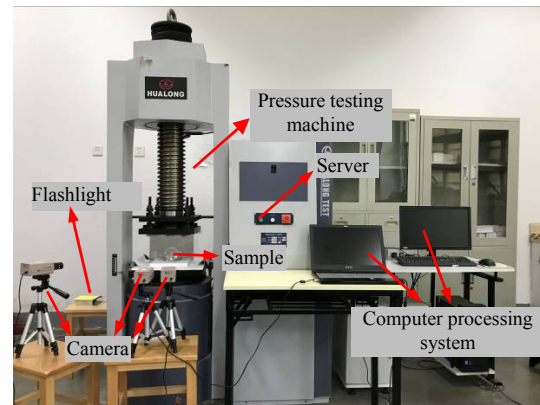


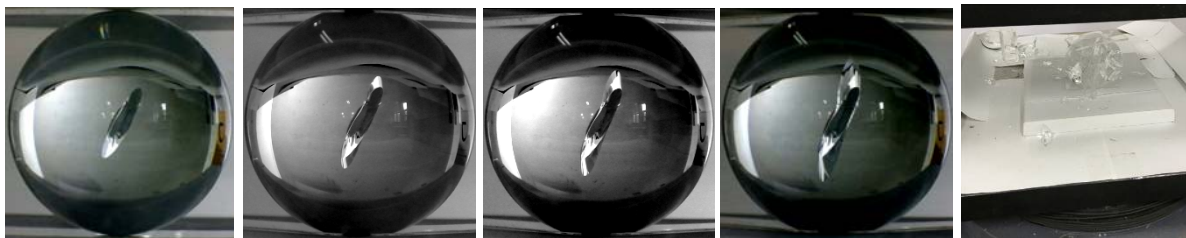
Fig.3 Loading system

3 Failure process and characteristics of stress moire

The process of crack propagation and failure of samples A1 and B1 in tests is shown in Fig. 4.



(a) Sample A1



(b) Sample B1

Fig.4 Failure process of sphere samples

3.1 Failure process of samples

(1) Samples without internal cracks (group A): as shown in Fig. 4(a), when the load reaches the failure load, the sample A1 bursts into tiny glass fragments and snow-like debris, which is the typical characteristic of brittle materials failure by a rigidity-testing machine.

(2) Samples with internal cracks (group B): as shown in Fig. 4(b), when the load reaches the initial cracking load, the crack grows at the upper and lower tips of the original crack simultaneously and expands to the vicinity of the load points at both ends with a certain initial cracking angle θ slowly and steadily.

Meanwhile, the original crack is wrapped and turns to a wing crack (upper and lower wing crack). The propagation rate obviously increases at the later stage. As the load reaches the failure load, the sample is penetrated by the surface of the main crack instantly.

3.2 Initiation of the internal crack and failure load of samples

As shown in Fig.5, the failure load for samples with a 60° internal crack is smaller than that for complete samples with an 87.07% decrease, indicating that the existence of the internal crack greatly reduces the sample strength. The ratio of initial cracking load to failure load is 21.31% for the sample with an internal crack.

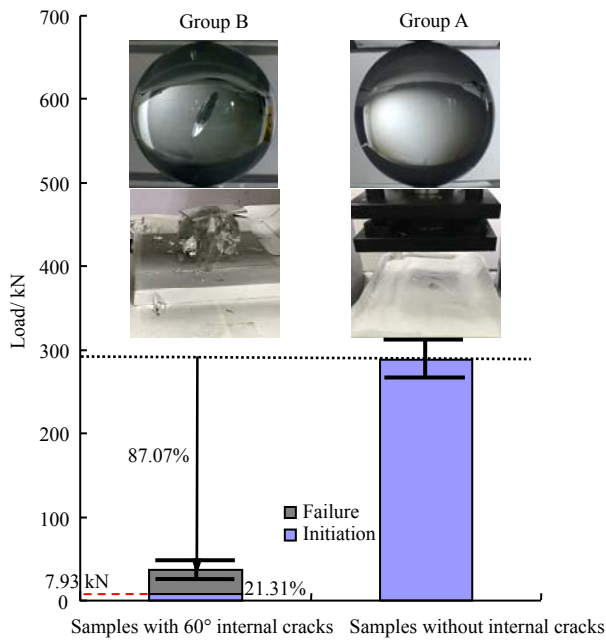


Fig.5 Initiation and failure loads

4 Characteristics of mode I-II-III fracture growth surface

As the load increases, the fracture firstly appears at the upper and lower tips of the original crack under compression-shear stress at a certain angle to the original crack surface, resulting in the typical growth of a wing crack. Figure 6 shows that the fracture growth trajectory is a "wrapping wing-shaped" curved surface.

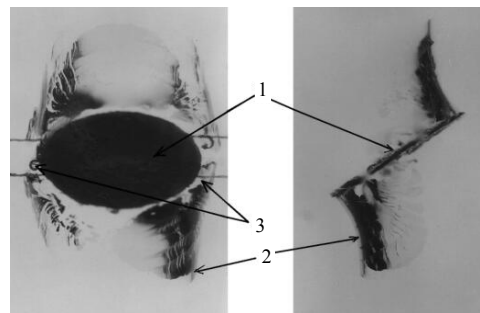
The fracture growth surface is divided into a smooth zone and a tear zone with different characteristics and mechanical mechanisms. Here, the fracture mode and the mechanism are illustrated based on the characteristics of the fracture growth surface in tests. The fracture mode will also be determined by the distribution of the intensity factor K at the crack tips calculated using M-integral in the following section.

4.1 Smooth zone (mode I-II fracture)

As shown in Fig.7, the crack growth surface is smooth and has rounded tips. The mode III fracture is not observed in the smooth zone based on the crack fractography (The crack growth surface with mode III fracture will be discussed with details in Section 4.2). A certain angle β can be witnessed between the fracture growth surface and the original crack surface, and the growth trajectory tends to be a gradual "wrapping wing-shaped" curved surface, implying that the fracture mode is I-II. For brittle materials, the brittle crack always grows in the direction that can minimize the shear load. When a mode II crack is superimposed, the brittle crack surface will slowly return to a stable plane perpendicular to the maximum principal tensile stress caused by an external field. The mode II field can be regarded as a "correction" to the crack deflection, and the crack finally turns from mode I-II to mode I^[30].

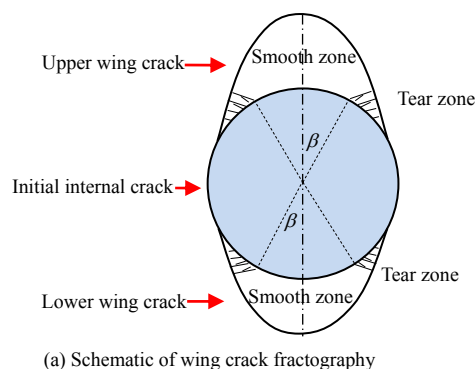


(a) Wing crack in our study (B)

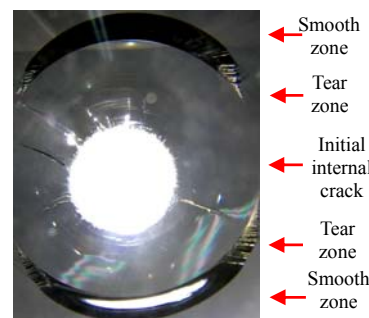
(b) Transparent rock-like wing crack casted by Dyskin et al. ^[16]

1—Initial internal crack
2—Wing crack
3—Petal-shaped crack

Fig.6 Growth of wing crack



(a) Schematic of wing crack fractography

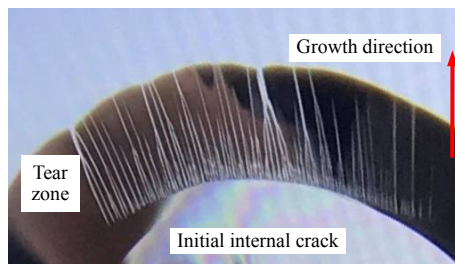


(b) Wing crack fractography from tests

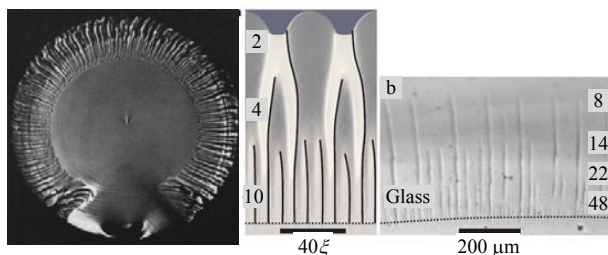
Fig.7 Partitions of wing crack fractography

4.2 Characteristics of the tear zone with mode III fracture

The tear zone in our study has a characteristic of the reverse binary tree and can be discontinuous as shown in Fig. 8(a) (The wing crack is rotated by 90°). Figure 8(b) displays the mode I-III fracture in literatures. The figure on the left has become the permanent cover of *Engineering Fracture Mechanics*^[31] and the figure on the right published in *Nature* is from numerical simulation of the mode I-III fracture^[32].



(a) Characteristics of the tear zone with mode III fracture in our study



(b) Characteristics of mode I-III fracture in literatures^[32–33]

(The right figure was published in *Nature*, and the values in the figure is the scale with a unit of μm .)

Fig.8 Cracks with mode III fracture

4.2.1 Reverse binary tree

(1) A dense linear distribution of fractures in the tear zone is observed near the tip of the original crack. As the crack extends outward, two or three lines converge and continue to extend, resulting in a thin linear distribution near the tip of the wing crack. Therefore, a reverse binary tree like the confluence of a river is witnessed.

(2) The tear zone is dislocated with a step-like side. Therefore, the model III fracture can also be observed in this area, leading to a combination of mode I, II, III fractures. This can also be confirmed by the calculated distributions of three stress intensity factors in the following section.

(3) Lines extend horizontally, indicating that the direction of the dislocation is along the u -axis of the original crack surface. Lines are thick near the boundary of the transition zone between upper and lower

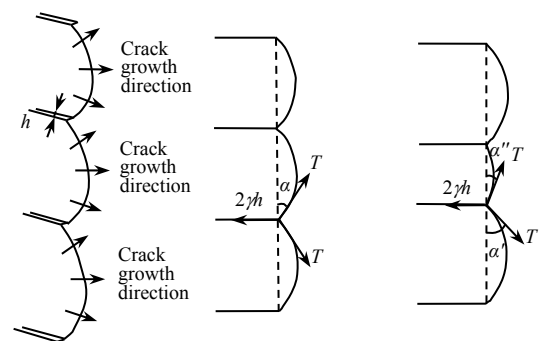
wing cracks, while they are thin at the edge.

For the crack in the shape of a reverse binary tree caused by the shear dislocation at the tip of the mode III fracture, Friedel^[33] gives the explanation theoretically: there is a linear tension T at the front tip of the crack, which is equal to the unit energy resulted from an increase in the crack front by a unit length. Additionally, T is assumed to be independent of the direction of the crack front and the speed of the crack. However, there is a drag force $2\gamma h$ at the step. γ represents the energy required to form a unit surface at the step and h is the height of the step. The schematic of the step cracks is shown in Fig. 9.

For equally spaced steps, the crack symmetrically bends and grows from the center of the step with $\alpha' = \alpha''$ (α' and α'' represent the angles between the left, right traction force and the direction perpendicular to the step, respectively). Then the condition for moving forward the entire crack front can be obtained:

$$2\gamma h = 2T \sin \alpha \quad (1)$$

where α is the angle between the traction force and the direction perpendicular to the step.



(a) Step cracks (b) Force balance (c) Causes of confluence

Fig.9 Schematic of step cracks and the causes of confluence phenomenon

If the spacing between the steps is unequal as shown in Fig. 9(c), there will be asymmetrical forces at the step ($\alpha' \neq \alpha''$, $T \sin \alpha' = T \sin \alpha''$). The steps with a small spacing will approach each other during the process of crack growth and these steps will merge into a new step. As the steps approach each other, the value of α'/α'' will increase, and the new and old step will further merge together. A binary tree is finally observed. However, such an ideal reverse binary tree pattern has not yet been witnessed.

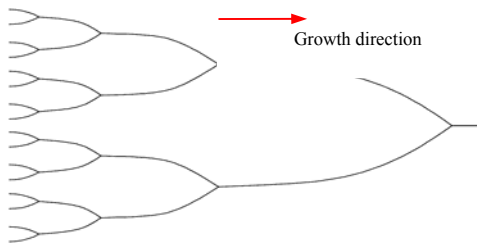


Fig.10 Ideal pattern for reverse binary tree

4.2.2 Incontinuity of mode III fracture initiation

It is worth noting that the thin line does not always extend from the tip of the original crack. The starting point of the edge of the partial tear zone does not coincide with the edge of the original crack in sample B1 (see dashed lines in Fig. 11(b)) and the incontinuity phenomenon can be observed. Therefore, there are only mode I-II fractures at the early stage of the wing crack propagation. The mode III fracture appears on the growth surface as the wing crack grows.

5 Damage form

5.1 Crack morphology

The fracture patterns include the upper wing crack, lower wing crack and primary crack. As shown in Fig.12, when the crack propagation comes to the late third stage (unsteady propagation), the sample is penetrated by both the primary crack and the wing crack at a high speed. The primary crack appears and grows from the surface near one of the upper and lower load points. After penetrating the original crack, it continues to extend to the surface of the sample on the other side. Meanwhile, wing cracks on both sides extend to the edge of the sample at an extremely high speed and meet with the primary crack. The surface of the primary crack tends to be flat and its normal direction is perpendicular to the direction of the force. The crack surface can be partially curved because of wing cracks, but it is still smooth.

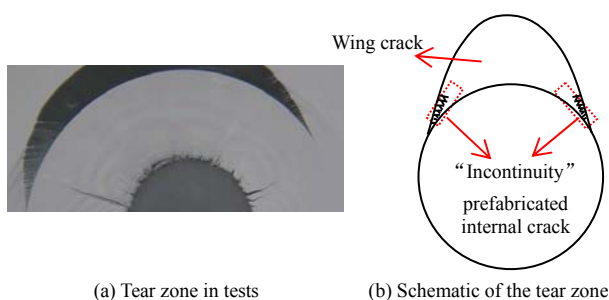


Fig.11 Incontinuity of the tear zone (Sample B1)

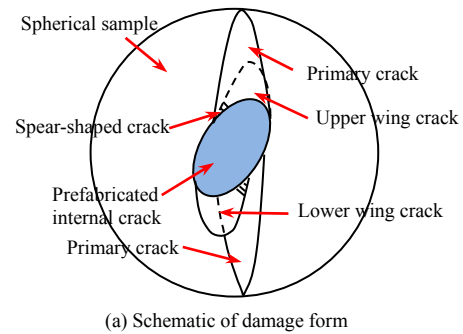


Fig.12 Schematic diagrams of damage form

5.2 Wedge-shaped part and impact failure

A wedge-shaped part is observed after tests as shown in Fig.13. Characteristics of a typical impact failure can be found in the fracture. It is speculated that the sample that is broken into two halves is still under stress at the moment when the primary crack penetrates the sphere. The primary crack and the wing crack are not coplanar, and the protruding part is instantaneously fractured. The wedge-shaped part falls out caused by the instantaneous impact. This article mainly focuses on static fracture mechanics and this phenomenon is a secondary damage that is in the category of dynamic fracture mechanics. Therefore, this phenomenon is discussed without thorough theoretical analysis.

(1) There is a boundary between the upper and lower wing cracks on the original crack surface, and the propagation of the primary crack always crosses this boundary. When the primary crack is close to the wing cracks, the primary crack partly bends and merges with the wing cracks, leading to a curved groove at the wing cracks. Then the primary crack and the wing cracks are overlapped and coplanar partly. However, when these cracks are not close to each other, a wedge will be

formed by independent crack surfaces, which can be divided into an upper wedge and a lower wedge.

(2) Either the upper wedge or the lower wedge is formed in our tests. However, when the primary crack is not close to both upper and lower wing cracks, these cracks will separate and not merge, resulting in two wedges.

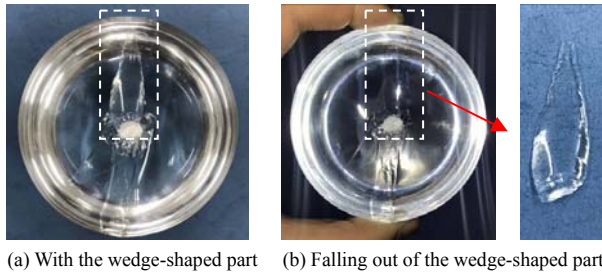


Fig.13 Wedge-shaped part

6 Numerical Simulation

6.1 Computational principle

Three stress intensity factors K_I , K_{II} and K_{III} are calculated by M-integral^[34]:

$$K_I = \frac{\mu\sqrt{2\pi}(x_b - x_a)}{\sqrt{r_{a-b}}(2 - 2x)} \quad (2)$$

$$K_{II} = \frac{\mu\sqrt{2\pi}(y_b - y_a)}{\sqrt{r_{a-b}}(2 - 2y)} \quad (3)$$

$$K_{III} = \frac{\mu\sqrt{2\pi}(z_b - z_a)}{\sqrt{r_{a-b}}} \quad (4)$$

where μ is the shear modulus; r_{a-b} is the distance between the crack tip and compute nodes; x_i , y_i and z_i are the displacements along the x -, y - and z -directions, respectively; $i = a, b$.

6.2 Computational model

Figure 14 displays the numerical model of the spherical sample with a 60° internal crack.

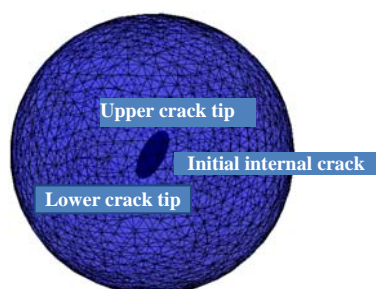


Fig.14 Numerical model

6.3 Results and comparisons with tests

The stress intensity factor is normalized using the absolute value of the maximum K , and the normalized stress intensity factor is defined as $K_m/|K_{\max}|$ ($m = I, II, III$). To directly show the partitions of the wing cracks, the absolute values of the normalized mode II and III stress intensity factors are calculated. The distributions of the three stress intensity factors are shown in Fig. 15 and compared with the test results in Fig. 16. In Fig. 15, 0 in abscissa represents the top of crack tip, 0.25 represents three o'clock position of crack tip, and 0.5 represents 6 o'clock position of crack tip.

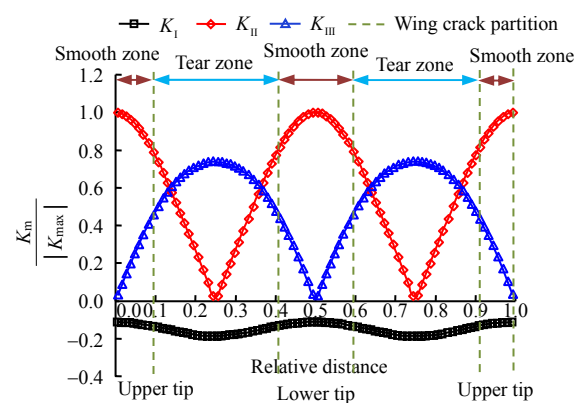


Fig.15 Distribution of $K_m/|K_{\max}|$ at crack front

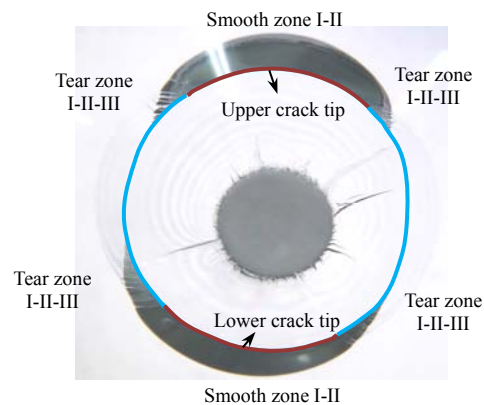


Fig.16 Test results of crack propagation

The initiation and propagation of cracks are analyzed based on the simulation and the test results:

(1) Initiation: the negative K_I indicates the crack-closing under pressure on the crack surface. The maximum K_{II} obtained at the upper and lower tips of the original crack shows that the dislocation is largest at the tips and the crack initiation under compression-shear stress is mainly caused by the mode II dislocation. After the initiation, the crack mode turns from II to I, which is consistent with analysis of the smooth

zone in tests.

(2) Propagation of the wing crack: a reverse binary tree pattern and the largest K_{III} is observed in the tear zones on both sides of the crack, indicating the existence of the mode III fracture. Therefore, the fracture in this zone is the combination of mode I, II and III. These findings are also consistent with the test results.

7 Conclusions

(1) The strength of a spherical sample with a 60° internal crack decreases by 87.07% compared with that of a complete sample. The fracture patterns include an upper wing crack, a lower wing crack and a primary crack. A wedge can be formed between the wing crack and the primary crack.

(2) The wing crack is composed of smooth zones (mode I-II fracture) and tear zones (mode I-II-III fracture). The fracture is in the shape of reverse binary tree.

(3) Based on the distributions of K_I , K_{II} and K_{III} at crack tips calculated by M-integral, the largest K_{II} is observed at the upper and lower tips because the crack initiation is caused by the mode II dislocation under the compression-shear stress. The largest K_{III} obtained at the tear zone indicates the existence of the mode III fracture. These results are consistent with tests.

(4) This study is an important supplement to the current research without considering internal cracks of spherical samples. 3D-ILC can be successfully applied to the investigation of spheres with internal cracks, and it provides an experimental and theoretical basis for the investigation of the mode I-II-III fracture in fracture mechanics.

References

- [1] ZHANG Le. The research on the ore crushing with high pressure grinding rolls based on discrete element method[D]. Xiangtan: Xiangtan University, 2016.
- [2] YI Jian-kun, MA Han-yu, ZHU Jian-sheng, et al. Analysis on scattering motion of explosive residue grains[J]. *Chinese Journal of Explosives & Propellants*, 2010, 33(5): 25–29.
- [3] GUO Xi-ling, HU Hui, BAO Cheng-gang. Effect of granular crushing of rockfill on dilatancy and shear strength[J]. *Chinese Journal of Geotechnical Engineering*, 1997, 19(3): 86–91.
- [4] SHEN Chao-min, LIU Si-hong. Evolution part for the particle breakage of granular materials: a micromechanical and thermodynamic insight[J]. *Chinese Journal of Theoretical and Applied Mechanics*, 2019, 51(1): 16–25.
- [5] JIAN Z, ZHANG L, PAN Z, et al. Numerical investigation of fluid-driven near-borehole fracture propagation in laminated reservoir rock using PFC^{2D}[J]. *Journal of Natural Gas Science & Engineering*, 2016, 36(5): 719–733.
- [6] XAVIER BRAJER, PASCAL FORQUIN, RENÉ GY, et al. The role of surface and volume defects in the fracture of glass under quasi-static and dynamic loadings[J]. *Journal of Non-Crystalline Solids*, 2003, 316(1): 42–53.
- [7] SALMAN A D, GORHAM D A. The fracture of glass spheres[J]. *Powder Technology*, 2000, 107(1): 179–185.
- [8] PERNAS-SÁNCHEZ J, ARTERO-GUERRERO J A, VARAS D, et al. Analysis of ice impact process at high velocity[J]. *Experimental Mechanics*, 2015, 55(9): 1669–1679.
- [9] CHEONG Y S, REYNOLDS G K, SALMAN A D, et al. Modelling fragment size distribution using two-parameter Weibull equation[J]. *International Journal of Mineral Processing*, 2004, 74(50): 227–237.
- [10] SHI Hong-shun. Study on fracture mechanism of brittle material based on peridynamics[D]. Guiyang: Guizhou University, 2017.
- [11] ZHU F, ZHAO J. A peridynamic investigation on crushing of sand particles[J]. *Géotechnique*, 2019, 69(6): 526–540.
- [12] MA G, ZHOU W, ZHANG Y, et al. Fractal behavior and shape characteristics of fragments produced by the impact of quasi-brittle spheres[J]. *Powder Technology*, 2018, 325(1): 498–509.
- [13] CHEN Xing, MA Gang, ZHOU Wei, et al. Effect of material disorder on impact fragmentation of brittle spheres[J]. *Acta Physica Sinica*, 2018, 67(14): 219–228.
- [14] GAO Yu-chen, ZHU Wei. Damage theory of materials with microcracks[J]. *Chinese Journal of Theoretical and Applied Mechanics*, 1987, 19(6): 541–549.
- [15] ADAMS M, SINES G. Crack extension from flaws in a brittle material subjected to compression[J]. *Tectonophysics*, 1978, 49(1–2): 97–118.
- [16] DYSKIN A V, JEWELL R J, JOER H E, et al. Experimental on three-dimensional crack growth in uniaxial compression[J]. *International Journal of Fracture*, 1994, 65(4): 77–83.
- [17] WANG H, DYSKIN A, PASTERNAK E, et al. Effect of the intermediate principal stress on 3-D crack growth[J]. *Engineering Fracture Mechanics*, 2018, 204(2): 404–420.
- [18] YANG Lei, MEI Jie, LI Shu-cai, et al. Research on the

- initiation and propagation moders of 3-D crack under hydro-mechanical coupling[J]. *Advanced Engineering Sciences*, 2018, 50(6): 174–183.
- [19] FU Jin-wei, ZHU Wei-shen, LUO Xiang-yu, et al. Study on fracture process of fracturerock by using a new material containing three-dimensional internal facture surfaces[J]. *Journal of Central South University (Science and Technology)*, 2014, 45(9): 3257–3263.
- [20] FU Jin-wei, ZHU Wei-shen, ZHANG Xin-zhong, et al. Fracturing experiment and numerical simulation study on new material containing a hollow internal cracks under internal water pressure[J]. *Advanced Engineering Sciences*, 2017, 49(4): 78–85.
- [21] JU Yang, XIE He-ping, ZHENG Ze-min, et al. Visualization method of complex structure and stress field of rock mass based on 3D printing technique[J]. *Chinese Science Bulletin*, 2014, 59(32): 3109–3119.
- [22] LIU Hua-bo. Crack propagation law of prefabricated flaw in rock like materials and the application of 3D printing technology[D]. Beijing: China University of Mining and Technology (Beijing), 2018.
- [23] WANG Hai-jun, ZHANG Jiu-dan, REN Ran, et al. Embedded cracks in brittle solids induced by laser-medium interaction (3D-ILC) [J]. *Chinese Journal of Geotechnical Engineering*, 2019, 41(12): 2345–2352.
- [24] WANG Hai-jun, YU Shu-yang, REN ran, et al. Study on failure of brittle solids with circular hole and internal crack based on 3D-ILC[J]. *Rock and Soil Mechanics*, 2019, 40(6): 2200–2212.
- [25] WANG Hai-jun, ZHANG Jiu-dan, REN Ran, et al. Fracture characteristics of Brazilian disc with fully internal cracks based on 3D-ILC[J]. *Chinese Journal of Geotechnical Engineering*, 2019, 41(9): 1636–1644.
- [26] WANG Hai-jun, LI Han-zhang, REN Ran, et.al. Study on the propagation law of internal crack and failure characteristics of three-point bending brittle solid based on 3D-ILC[J]. *Chinese Journal of Rock Mechanics and Engineering*, 2019, 38(12): 2463–2477.
- [27] Li Shi-yu. *Introduction of rock fracture mechanics*[M]. Hefei: University of Science and Technology of China Press, 2010.
- [28] GRIFFITH A A. The phenomena of rupture and flow in solids[J]. *Philosophical Transactions of the Royal Society of London*, 1921, 221(2): 163–198.
- [29] DEREK HULL. *Fractography: observing, measuring and interpreting fracture surface topography*[M]. Cambridge: Cambridge University Press. 1999.
- [30] BRIAN LAWN. *Fracture of brittle solids*[M]. Cambridge: Cambridge University Press, 1993.
- [31] SOMMER E. Formation of fracture “lances” in glass[J]. *Engineering Fracture Mechanics*, 1969, 1(3): 539–546.
- [32] PONS A J, KARMA A. Helical crack-front instability in mixed-mode fracture[J]. *Nature*, 2010, 464(7285): 85–89.
- [33] FRIEDEL J. Propagation of cracks and work hardening[J]. *Independent on Sunday*, 2012, 314(12): 558–565.
- [34] SUN Xin, ZHU Zhi-ming, XIE Ling-zhi, et al. Investigation on mixed-mode fracture behavior of sand stone using a SENDB specimen[J]. *Chinese Journal of Rock Mechanics and Engineering*, 2017, 36(12): 2884–2894.